Detections of Nearly Bias-free Core Shifts with 5-30 μas Precisions at 8-43 GHz in BL Lacertae

Downloaded from: https://research.chalmers.se, 2026-10-07 19:34 UTC

Citation for the original published paper (version of record):
Liu, N., Yang, J., Cheng, X. et al (2026). Detections of Nearly Bias-free Core Shifts with 5-30 μas Precisions at 8-43 GHz in BL Lacertae. Astrophysical Journal, 1003(1).
http://dx.doi.org/10.3847/1538-4357/ae63b4

N.B. When citing this work, cite the original published paper.

research.chalmers.se offers the possibility of retrieving research publications produced at Chalmers University of Technology. It covers all kind of research output: articles, dissertations, conference papers, reports etc. since 2004. research.chalmers.se is administrated and maintained by Chalmers Library

(article starts on next page)

The Astrophysical Journal, 1003:54 (11pp), 2026 May 20 https://doi.org/10.3847/1538-4357/ae63b4
© 2026. The Author(s). Published by the American Astronomical Society.
OPEN ACCESS

Detections of Nearly Bias-free Core Shifts with 5–30 μas Precisions at 8–43 GHz in BL Lacertae

Niu Liu (刘牛)[1,2], Jun Yang (杨军)[3], Xiaopeng Cheng (程晓朋)[4], Ai-Ling Zeng (曾艾玲)[5], Wen Chen (陈文)[6], Xiao-Long Yang (杨小龙)[7], Xiaoyu Hong (洪晓瑜)[7,8], Xia-Xuan Zhang (张夏轩)[1,2], Jia-Cheng Liu (刘佳成)[1,2], and Zi Zhu (朱紫)[1,2,9]

[1] School of Astronomy and Space Science, Nanjing University, Nanjing 210023, People's Republic of China; niu.liu@nju.edu.cn
[2] Key Laboratory of Modern Astronomy and Astrophysics (Ministry of Education), Nanjing University, Nanjing 210023, People's Republic of China
[3] Department of Physics and Astronomy, Chalmers University of Technology, Onsala Space Observatory, SE-43992 Onsala, Sweden; jun.yang@chalmers.se
[4] Korea Astronomy and Space Science Institute, 776 Daedeok-daero, Yuseong-gu, Daejeon 34055, Republic of Korea; xcheng@kasi.re.kr
[5] Instituto de Astrofísica de Andalucía-CSIC, Glorieta de la Astronomía s/n, E-18008 Granada, Spain
[6] Yunnan Observatories, Chinese Academy of Sciences, Yangfangwang 396th, Kunming, People's Republic of China
[7] Shanghai Astronomical Observatory, Chinese Academy of Sciences, Shanghai 200030, People's Republic of China
[8] University of Chinese Academy of Sciences, Beijing 100049, People's Republic of China
[9] University of Chinese Academy of Sciences, Nanjing 211135, People's Republic of China
Received 2026 February 13; revised 2026 April 14; accepted 2026 April 21; published 2026 May 14

Abstract

When a radio jet is partially optically thick in the launching region, its apparent compact core may display frequency-dependent positional shifts. High-precision astrometric measurements of core shifts enable astronomers to pinpoint the jet's origin and place tight constraints on the magnetic field. BL Lacertae, the archetypal BL Lac object, hosts a highly variable and well-collimated jet. To independently constrain its innermost core shifts, we conducted very long baseline interferometric (VLBI) observations at 8.4, 12.4, 15.2, 23.6, and 43.2 GHz. By exploiting a nearby (13.′3) steep-spectrum calibrator (NVSS J220340+420839) through inverse phase-referencing VLBI astrometry, we detect nearly unbiased two-dimensional core shift measurements with state-of-the-art precisions of 5–30 μas, which are significant at $>3\sigma$ confidence. The core shift between 8.4 and 43.2 GHz reaches 250 μas. The apparent core shifts scale with frequency as ν^{-1/k_r}, implying the existence of an optically thick region in the upstream of the jet. The derived core-shift index, $k_r = 1.18^{+0.59}_{-0.34}$, is consistent, within uncertainties, with the canonical $k_r = 1$ expected under energy equipartition between the jet particle and magnetic field energy densities, while allowing for modest deviations given that BL Lacertae was captured in a flaring state.

Unified Astronomy Thesaurus concepts: BL Lacertae objects (158); Relativistic jets (1390); Extragalactic magnetic fields (507); Radio continuum emission (1340); Very long baseline interferometry (1769); Astrometry (80)

1. Introduction

Blazars are the most highly variable class of radio-loud active galactic nuclei, whose emission is dominated by relativistic jets oriented at small angles to the line of sight and strongly affected by Doppler boosting. Relativistic jets are thought to be launched through the interaction between a supermassive black hole (SMBH) and parsec-scale magnetic fields in the surrounding accretion flow (A. P. Marscher et al. 2008). Magnetic field is expected to play a key role in governing jet propagation, particularly within the inner jet acceleration and collimation region. Under some astrophysical jet models, the magnetic field near SMBHs can be properly probed with high-resolution very long baseline interferometry (VLBI) observations.

On the VLBI map, the radio core is typically identified as the location where the optical depth due to synchrotron self-absorption approaches unity (R. D. Blandford & A. Königl 1979). Its apparent position therefore depends on observing frequencies, with lower-frequency cores appearing farther downstream than those observed at higher frequencies, following $r \propto \nu^{-1/k_r}$. This frequency-dependent displacement of the radio core, known as the core shift, provides an effective probe of physical conditions in the innermost jet (A. Konigl 1981; A. P. Lobanov 1998; S. P. O'Sullivan & D. C. Gabuzda 2009). Previous core-shift measurements have often yielded power-law indices k_r (also known as the core-shift index) close to unity (S. P. O'Sullivan & D. C. Gabuzda 2009; K. Hada et al. 2011; K. V. Sokolovsky et al. 2011), broadly consistent with a freely expanding conical jet under near-equipartition between particle and magnetic energy densities (A. P. Lobanov 1998). Recent studies have found that core-shift variability is common in active galactic nuclei and may be associated with nuclear flares that inject denser plasma into the jet (A. V. Plavin et al. 2019; W. Chamani et al. 2023). If the radio core includes a strong standing shock, the core positions at high frequencies might converge toward the shock location, resulting in little or no measurable core shift (A. Marscher 2010). Consequently, the core-shift effect could help search for standing shocks in the inner jet region.

BL Lacertae is one of the best BL Lac objects for studying jet astrophysics close to SMBHs thanks to its proximity ($z = 0.0655$; M. J. Koss et al. 2022) and brightness. High-angular-resolution VLBI observations reveal a bright core and a one-sided jet extending southward, with two stationary features near the core (A. P. Marscher et al. 2008; J. L. Gómez et al. 2016;

Original content from this work may be used under the terms of the Creative Commons Attribution 4.0 licence. Any further distribution of this work must maintain attribution to the author(s) and the title of the work, journal citation and DOI.

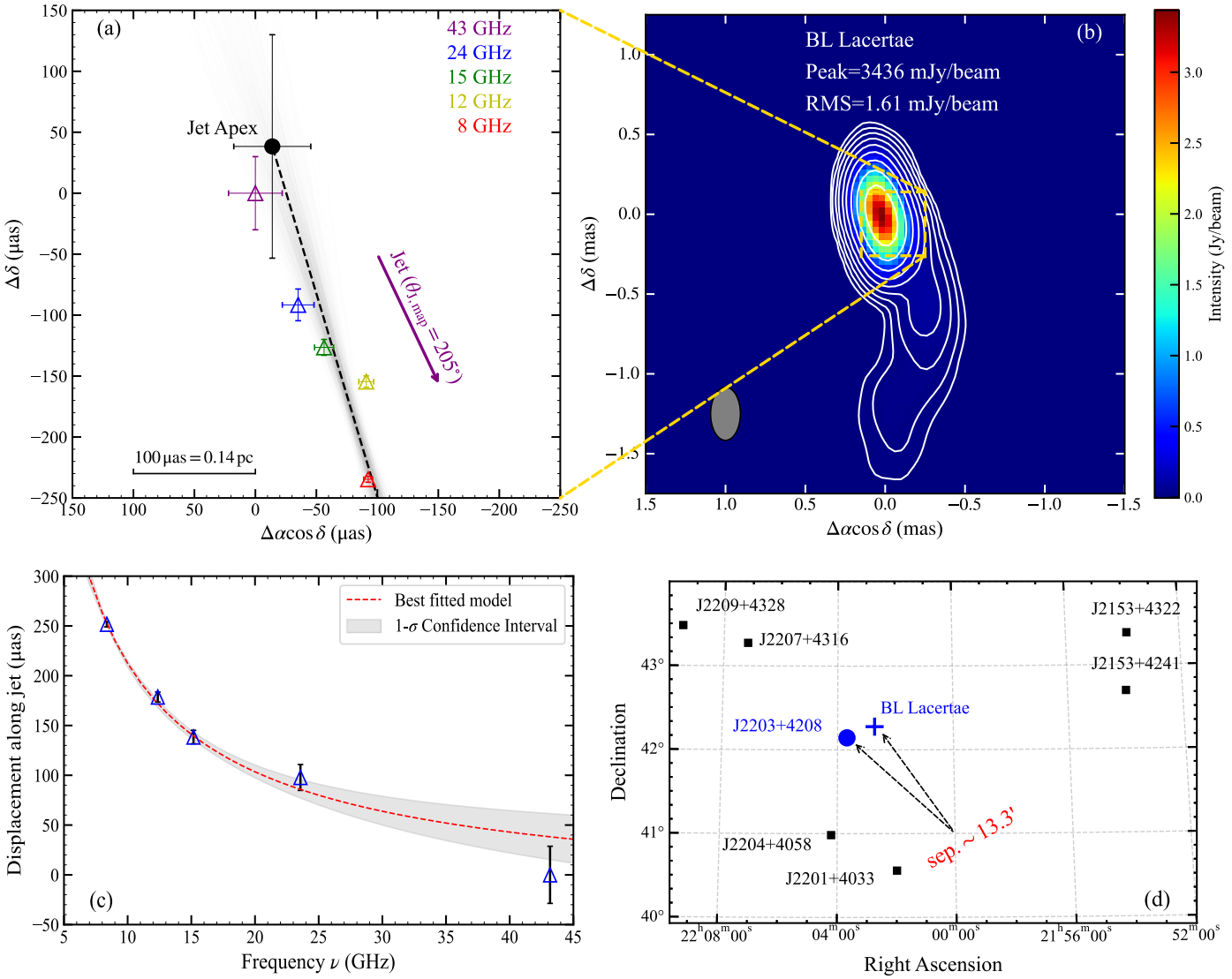

Figure 1. Core-shift measurements of BL Lacertae. (a) Two-dimensional core shifts at 8.4, 12.4, 15.2, and 23.6 GHz relative to 43.2 GHz. The dashed line denotes the best-fit core-shift model, and the gray region shows the scatter from 1000 randomly sampled MCMC realizations. (b) 43 GHz VLBA image. (c) Projected core displacements along the jet direction, adopting a position angle of 197°. The red dashed line shows the best-fit model prediction, with the gray region indicating the 1σ confidence interval. (d) Calibrator field around BL Lacertae. Black squares mark six sources from the Radio Fundamental Catalog (rfc_2025c; L. Y. Petrov & Y. Y. Kovalev 2025), and the blue circle indicates the reference calibrator used in this work.

C. Casadio et al. 2021) when there are no giant flares. The jet structure of BL Lacertae is, however, known to be highly variable with time, particularly during episodes of strong flaring activity (S. G. Jorstad et al. 2022). Using a two-dimensional cross-correlation alignment based on the optically thin jet emission in multifrequency VLBI images, S. P. O'Sullivan & D. C. Gabuzda (2009) measured significant core shifts (40–460 μas) between 4.6 and 43.1 GHz, consistent with expectations from the standard conical jet model. In addition, source-frequency phase-referencing VLBI observations reported a much smaller core shift of only $\sim$20 μas between 22 and 43 GHz during a long-lived giant flare, possibly resulting from a recollimation shock in the inner region (R. Dodson et al. 2017). Recently, we have identified a compact, steep-spectrum source at an angular separation of only $\sim$13.′3 from BL Lacerate in two pilot experiments, including a Very Long Baseline Array (VLBA) experiment (project code: TC031; PI: Jun Yang) at 22 and 43 GHz and a European VLBI Network (EVN) experiment (project code: RSY08; PI: Jun Yang) at 5 GHz. This enables us to gain more accurate differential calibration of atmospheric and instrumental phase errors (M. J. Rioja & R. Dodson 2020) and provides independent, nearly unbiased measurements of core shifts in BL Lacertae.

This paper is organized as follows. Section 2 describes the VLBI observations and data reduction. Section 3 presents the multifrequency differential astrometry results for BL Lacertae. We compare our results with previous studies to constrain the nature of the jet magnetic field in Section 4. Finally, we summarize our conclusions in Section 5. For a flat universe with $\Omega_m = 0.315$, $\Omega_\Lambda = 0.811$, and $H_0 = 67.4$ km s^{-1} Mpc^{-1} (Planck Collaboration et al. 2020), the redshift of BL Lacertae corresponds to a luminosity distance $D_L = 305.59$ Mpc, and 1 mas corresponds to 1.39 pc.

2. Observations and Data Reduction

We observed BL Lacertae and the reference source NVSS J220340+420839 (hereafter J2203+4208) with the

VLBA (project code: BY 196; PI: Jun Yang) on 2024 July 27 in a phase-referencing observation mode at five frequencies: 8.4, 12.4, 15.2, 23.6, and 43.2 GHz. All VLBA antennas participated except Los Alamos. We followed a standard US National Radio Astronomy Observatory (NRAO) Astronomical Image Processing System (AIPS, version 31DEC25) procedure to calibrate visibility data at all bands, using BL Lacertae as a fringe finder and bandpass calibrator. After preliminary calibration, BL Lacertae was imaged in DIFMAP (version 2.5q). The source models (CLEAN components) determined from the BL Lacertae images were exported to AIPS and used as the input model to derive self-calibration solutions (phase and amplitude), which were applied to both BL Lacertae and J2203+4208. The details of observational strategy, experiment setup, and calibration procedure are summarized in Appendix A.

The calibrated visibilities of J2203+4208 were then split and imaged in DIFMAP with natural weighting. A single circular Gaussian component was fitted to the target using MODELFIT, yielding the integrated flux density and the component position relative to the phase center (Appendix B). BL Lacertae shows a compact, one-sided core-jet morphology oriented roughly north–south, which is core dominated (Figure 1). The core position of BL Lacertae is defined as the location of the peak on the maps, for which nonzero offsets relative to the image origin (correlator phase center) were accounted for by model fitting with a single elliptical Gaussian component to the core region using JMFIT in AIPS (Appendix B). Subtracting this BL Lacertae core positional offset from position offsets of J2203+4208 aligns cores of BL Lacertae across frequencies onto a common local reference frame and provides core-shift measurements.

3. Multifrequency Differential Astrometry on BL Lacertae

3.1. Radio Spectrum of J2203+4208

The reference source J2203+4208 was firmly detected at all five frequencies. At frequencies of 23.6 GHz and below, the signal-to-noise ratios (SNRs) on the dirty maps exceeded 13, while the SNR was approximately 5.5 at 43.2 GHz. The frequency dependence of the integrated flux densities obtained from the model fitting is shown in Appendix B. A standard nonthermal power-law model was used to fit the spectrum of J2203+4208, in which the flux density S_ν at frequency ν is expressed as

$$S_\nu(\nu) = S_0 \cdot \nu^\alpha, \tag{1}$$

where S_0 is the amplitude of the synchrotron spectrum and α is the spectral index. The fitting yielded $\alpha = -1.27 \pm 0.02$, indicating a steep spectrum of J2203+4208. Therefore, J2203+4208 is optically thin and hence not subject to any detectable core shift, making it a reliable reference source for measuring the core shift of nearby targets.

3.2. Nearly Unbiased Core-shift Measurements

The relative positional offsets of J2203+4208 were determined with a precision of $\leqslant 7$ μas at frequencies lower than 15.2 GHz, 13 μas at 23.6 GHz, and approximately 30 μas at 43.2 GHz. During our observations, the mean zenith angle of J2203+4208 and BL Lacertae is 27° at 43.2 GHz and ranges from 40° to 50° at other frequencies. Taking into account a residual tropospheric zenith excess path length of 3 cm, as adopted in M. J. Rioja & R. Dodson (2020), the systematic errors due to extrapolation of phase-referencing solutions are all below 5 μas and thus can be reasonably omitted in the following analyses. Assuming that the position of J2203+4208 does not change with frequency, we aligned the positions of the innermost core of BL Lacertae onto the 43 GHz map and determined the core shift of BL Lacertae, as presented in Table 1. We also measured the position angle of the jet direction (counted from north to east) using the 43 GHz calibrated visibilities of BL Lacertae by MODELFIT. The position angle of the first elliptical Gaussian component was adopted, which gives $\theta_{\rm J,map} = 205\overset{\circ}{.}36 \pm 0\overset{\circ}{.}01$. As shown in Figure 1, the core positions of BL Lacertae at five frequencies roughly align, which is nearly parallel to the direction of the jet.

Table 1
Core-shift Measurements for BL Lacertae

Freq. (GHz)	$\Delta\alpha^*$ (μas)	$\Delta\delta$ (μas)	Shift (μas)	PA (deg)
		43.2 GHz core as origin		
8.4	-92 ± 4	-235 ± 2	253 ± 29	202 ± 5
12.4	-91 ± 6	-155 ± 5	181 ± 28	210 ± 8
15.2	-56 ± 8	-126 ± 7	141 ± 29	204 ± 11
23.6	-35 ± 13	-92 ± 13	102 ± 31	201 ± 17
43.2	0 ± 22	0 ± 30	...	...
		23.6 GHz core as origin		
8.4	-57 ± 4	-143 ± 2	155 ± 13	202 ± 5
12.4	-56 ± 6	-63 ± 5	85 ± 14	222 ± 10
15.2	-21 ± 8	-35 ± 7	44 ± 14	211 ± 22
		15.2 GHz core as origin		
8.4	-36 ± 4	-108 ± 2	114 ± 7	198 ± 4
12.4	-35 ± 6	-28 ± 5	45 ± 9	231 ± 12
		12.4 GHz core as origin		
8.4	-2 ± 4	-80 ± 2	80 ± 5	181 ± 5

Note. The formal uncertainties of $\Delta\alpha^* = \Delta\alpha \cos\delta$ and $\Delta\delta$ represent the positional uncertainties of core at each individual frequency for BL Lacertae, while the computation of formal uncertainties in shift and position angle (PA) have taken the positional uncertainties at both frequencies into consideration.

We adopted a two-dimensional model to describe the core shift at the observing frequency ν as

$$\begin{aligned} \Delta\alpha\cos\delta &= x_0 + r_0 \cdot \nu^{-\kappa} \sin\theta_{\rm J}, \\ \Delta\delta &= y_0 + r_0 \cdot \nu^{-\kappa} \cos\theta_{\rm J}, \end{aligned} \tag{2}$$

where r_0 and $\kappa = 1/k_r$ are core-shift parameters, and θ_J is the core-shift direction counted from north to east. The coordinate (x_0, y_0) of the jet apex can also be directly inferred from the multifrequency relative astrometric measurements without an assumed jet direction. We fitted the observed astrometric position offsets with the physical core-shift model given in Equation (2) and determined the posterior distributions of the parameters (r_0, k_r, x_0, y_0, θ_J) with a Markov Chain Monte Carlo (MCMC) sampler. This approach accounts for the nonlinear nature of the model and strong covariances among parameters (Appendix C). The fit returned

$$\begin{aligned} &r_0 = 1726^{+1123}_{-425}\ \mu\text{as}, \quad k_r = 1.18^{+0.59}_{-0.34}, \\ &x_0 = -14^{+34}_{-21}\ \mu\text{as}, \quad y_0 = 38^{+100}_{-60}\ \mu\text{as}, \\ &\theta_{\rm J} = 197^\circ \pm 3^\circ. \end{aligned} \tag{3}$$

This estimate of direction of the core shift aligns well with the average value of 14° ± 10° reported by S. P. O'Sullivan & D. C. Gabuzda (2009). The apparent difference reflects the fact

the position angles are defined modulo 180°; our value of 197° is equivalent to 17° and is consistent within the formal uncertainties.

4. Discussion

The projected core shifts of 30 to 180 μas (typical uncertainty of 20–40 μas) relative to 43.1 GHz determined in S. P. O'Sullivan & D. C. Gabuzda (2009) are slightly smaller than our measurements, but remain consistent within the formal uncertainties. A. B. Pushkarev et al. (2012) measure core shifts in 2006 with position angles of ∼180°. While the core shift of ∼70 to ∼130 μas between 8.4 and 15.4 GHz encompasses our value (114 ± 7 μas), their shift between 12.1 and 15.4 GHz (124–160 μas) is significantly larger than our measurement of 45 ± 9 μas. R. Dodson et al. (2017) report a shift of approximately 20 μas between 22 and 43 GHz, which is significantly smaller than the prediction of the core-shift model. We measure a shift of approximately 100 μas between 23.6 and 43.2 GHz with a $>3\sigma$ confidence. We note that our observations coincided with a strong flaring state of BL Lacertae. A further inspection of the MOJAVE (15 GHz)[10] and BEAM-ME (43 GHz)[11] light curves reveals that previous results correspond to different activity states compared to the strong flare seen in our data, likely explaining the discrepancies. Similar variability-dependent core-shift behavior has also been observed in other sources (e.g., A. V. Plavin et al. 2019). Since the frequency dependence of the measured core shifts in our data is well described by the core-shift model, we conclude that the 43 GHz core observed in our experiment corresponds to an optically thick component.

For an equipartition state between the jet particle and magnetic field energy densities, the core-shift index is expected to be $k_r = 1$. Previous reported values are generally consistent with this assumption, including $k_r = 0.99 \pm 0.07$ from S. P. O'Sullivan & D. C. Gabuzda (2009) and $k_r = 1.06 \pm 0.22$ in A. Agarwal et al. (2017) derived from radio light curves at five frequencies between 4.8 and 36.8 GHz spanning more than 40 yr. The derived value of the core-shift index of 1.18 remains higher, but is still consistent with this assumption, considering the formal uncertainty. The excess may be caused by the flare, as observed in 3C 345.3 (W. Chamani et al. 2023).

We calculate the magnetic field strength from the core-shift measurements following S. P. O'Sullivan & D. C. Gabuzda (2009), using the revised formula from W. Chamani et al. (2023). The jet kinematic parameters are taken from S. G. Jorstad et al. (2005), including the jet viewing angle of $7\overset{\circ}{.}7$, the Doppler factor of 7.2, and the half-opening angle of the jet of $1\overset{\circ}{.}9$. Adopting $k_r = 1$ yields a core magnetic field strength $B_{\rm core}(\nu)$ ranging from 0.06 ± 0.01 G at 8.4 GHz to 0.26 ± 0.05 G at 43.2 GHz. This corresponds to a magnetic field strength at 1 pc of $B_1 = 0.134 \pm 0.006$ G, roughly consistent with $B_1 = 0.139$ G in S. P. O'Sullivan & D. C. Gabuzda (2009), while greater than 0.09 G given in M. Zamaninasab et al. (2014). Alternatively, using $k_r = 1.18$ yields slightly lower high-frequency magnetic fields (0.23 ± 0.03 G at 43.2 GHz), resulting in a higher magnetic field strength at 1 pc of $B_1 = 0.201 \pm 0.010$ G. Based on these results, we predict an 86 GHz core magnetic field strength of 0.32 G (for $k_r = 1.18$) to 0.42 G (for $k_r = 1$).

While the core-shift measurements broadly follow the jet direction, we notice a small deviation from a strictly linear, one-dimensional trend in Figure 1. Given the high phase-referencing precision of our measurements, this nonlinear alignment may reflect the intrinsic structure (e.g., jet bending) or the frequency-dependent opacity effects coupled with variations in the jet direction (i.e., jet precession) of BL Lacertae. Further multifrequency observations would be required to confirm its astrophysical origin.

We also note that the calibrator, J2203+4208, exhibits a tentative jetlike extension toward the north (Appendix B), which could potentially introduce systematic astrometric shifts due to core-jet blending. To quantify this effect, we performed a trial reanalysis by introducing an additional component to represent the possible jet emission. The resulting change in the relative core position of BL Lacertae is found to be less than 30 μas in both R.A. and decl. This structural blending is most pronounced at 8.4 GHz, whereas no such feature is apparent at 23.6 and 43.2 GHz. Rederiving the core-shift parameters via MCMC fitting with these updated positions yielded results fully consistent with our primary analysis within the formal uncertainties. Therefore, we conclude that the impact of core-jet blending in the calibrator is negligible and does not affect our conclusions. Further dedicated VLBI observations at lower frequencies would help to confirm the nature of this tentative feature of the calibrator.

5. Conclusion

We present, for the first time, two-dimensional core-shift measurements at the precisions of 5 to 30 μas for BL Lacertae between 8.4 and 43.2 GHz, obtained using the inverse phase-referencing technique. This straightforward approach enables us to derive nearly bias-free core-shift measurements, particularly between 23.6 and 43.2 GHz, owing to the small angular separation of approximately 13′ between BL Lacertae and the reference steep-spectrum source (approximately an order of magnitude smaller than in previous studies). These results are entirely independent of earlier work and provide new constraints on the physical conditions of the jet in BL Lacertae during its flaring state.

Acknowledgments

N.L. and J.C.L. were supported by the National Natural Science Foundation of China (NSFC) under grant Nos. 12573070 and 12373074. W.C. was supported by the National Natural Science Foundation of China (NSFC) under grant No. 12573073, Yunnan Fundamental Research Projects (grant No. 202401AT070144), and Yunnan Foreign Talent Introduction Program (grant No. 202505AO120021). X.C. was supported by the Brain Pool Program through the National Research Foundation of Korea (NRF) funded by the Ministry of Science and ICT (RS-2024-00407499). This research was supported by the National Research Foundation of Korea (NRF) funded by the Korea government (KASA, Korea AeroSpace Administration; grant Nos. RS-2024-00509838 and R25TA0065942000). This work used data from the MOJAVE database, which is maintained by the MOJAVE team (M. L. Lister et al. 2018), and the Radio Fundamental Catalog (rfc_2025c) with the associated dataset available at NASA

[10] https://www.cv.nrao.edu/MOJAVE/sourcepages/2200+420.shtml
[11] https://www.bu.edu/blazars/VLBA_GLAST/bllac.html

(L. Petrov 2024). This work also uses VLBA data from the VLBA-BU Blazar Monitoring Program (BEAM-ME and VLBA-BU-BLAZAR; http://www.bu.edu/blazars/BEAM-ME.html), funded by NASA through the Fermi Guest Investigator Program. The VLBA is an instrument of the National Radio Astronomy Observatory. The National Radio Astronomy Observatory is a facility of the National Science Foundation operated by Associated Universities, Inc. The European VLBI Network is a joint facility of independent European, African, Asian, and North American radio astronomy institutes. The scientific results from the data presented in this publication are derived from the following EVN project code(s): RSY08. This work benefited from the Box, LaTeX, and Git services provided by the e-Science Center of the Collaborative Innovation Center of Advanced Microstructures, Nanjing University. The Jupyter Notebook to generate the figures in this paper is hosted at https://git.nju.edu.cn/astrometry/bllac_core_shift and is preserved on Zenodo at doi:10.5281/zenodo.19691949.

Facility: VLBA (NRAO).

Software: AIPS (E. W. Greisen 2003), DIFMAP (M. C. Shepherd 1997), `astropy` (Astropy Collaboration et al. 2013, 2018, 2022), `numpy` (S. Van Der Walt et al. 2011), `SciPy` (P. Virtanen et al. 2020), `emcee` (D. Foreman-Mackey et al. 2013), `matplotlib` (J. D. Hunter 2007), Jupyter Notebook (T. Kluyver et al. 2016).

Appendix A
Observation Strategy and Calibration Process

Thanks to the small angular separation of approximately 13.′3 between BL Lacertae and J2203+4208, we allocated 18 s for the switching between sources in each cycle. The duration times were approximately 1 hr at 8.4 GHz, 1 hr at 12.4 GHz, 1 hr at 15.2 GHz, 2 hr at 23.6 GHz, and 6 hr at 43.2 GHz (11 hr total). Table 2 summarizes the nodding cycle times and observational setup.

Data were recorded in dual polarization at 4096 Mb s^{-1} with 2-bit quantization, using 4 × 128 MHz sub-bands per polarization. Correlation was performed with the DiFX software correlator in Socorro, New Mexico, using 0.5 s integration and 0.5 MHz spectral channels. The correlation position was set to R.A. = $22^h02^m43\overset{s}{.}2914$, decl.=+42°16′39.″980 for BL Lacertae and to R.A. = $22^h03^m40\overset{s}{.}6110$, decl.=+42°08′39.″419 for J2203+4208, the latter having been determined from a VLBA testing observation experiment (project code: TC031; PI: Jun Yang) at 23.6 and 43.2 GHz and an EVN short observation (project code: RSY08; PI: Jun Yang) at 4.9 GHz.

The calibration followed the standard AIPS procedures and was identical at all bands. Ionospheric dispersive delays were corrected via global total electron content maps derived from Global Navigation Satellite System data. The residual delays due to inaccurate a priori values of Earth orientation parameters (EOPs) were corrected using the standard rapid EOP solutions from the International Earth Rotation and Reference Systems Service. Phase terms from antenna parallactic angle variations were removed. Instrumental single-band delays and phase offsets were determined from a dedicated 2 minute scan of BL Lacertae and applied to all scans. The bandpass responses were derived from the BL Lacertae scans, averaging in time over the full track and in frequency within each 128 MHz sub-band; one solution per intermediate frequency (IF) and polarization was applied. A priori amplitude calibration used the measured system temperatures and antenna gain curves recorded at each station during the run. After data inspection and flagging, global fringe fitting was performed on BL Lacertae with a 10 s solution interval at 8.4–23.6 GHz and 5 s at 43.2 GHz, using a point-source model and averaging across all sub-bands. Phase solutions from BL Lacertae were then transferred to J2203+4208 via linear interpolation in time.

After preliminary calibration, the visibility data of BL Lacertae were exported, after flagging 32 edge channels (25%), and then imaged in DIFMAP. The source models of BL Lacertae were exported to AIPS and used as the input model to derive self-calibration solutions. These solutions were applied to both BL Lacertae and J2203+4208. The left panel of Figure 2 presents the final phase solutions for all stations at 43.2 GHz during the first observing hour. The rapid phase variations of the VLBA-OV (Owens Valley) station are observed at all five frequencies, which are likely to be caused by the residual clock rate after correlation. The right panel shows the residual phases for BL Lacertae after applying the final phase solutions at 43.2 GHz over the same time interval, demonstrating small phase residuals.

Table 2
Nodding Cycle Times, On-source Scan Lengths, and Total On-source Integration Times for BL Lacertae (BL Lac) and J2203+4208 (J2203)

Freq. (GHz)	Nodding Cycle (minutes)	On-source Scan		Total On-source Time	
		BL Lac (s)	J2203 (s)	BL Lac (minutes)	J2203 (hr)
8.4	4	10	210	4.0	1.05
12.4	3	10	150	7.5	0.92
15.2	3	10	150	7.5	0.83
23.6	2	25	90	12.5	1.25
43.2	1	5	40	31.9	3.72

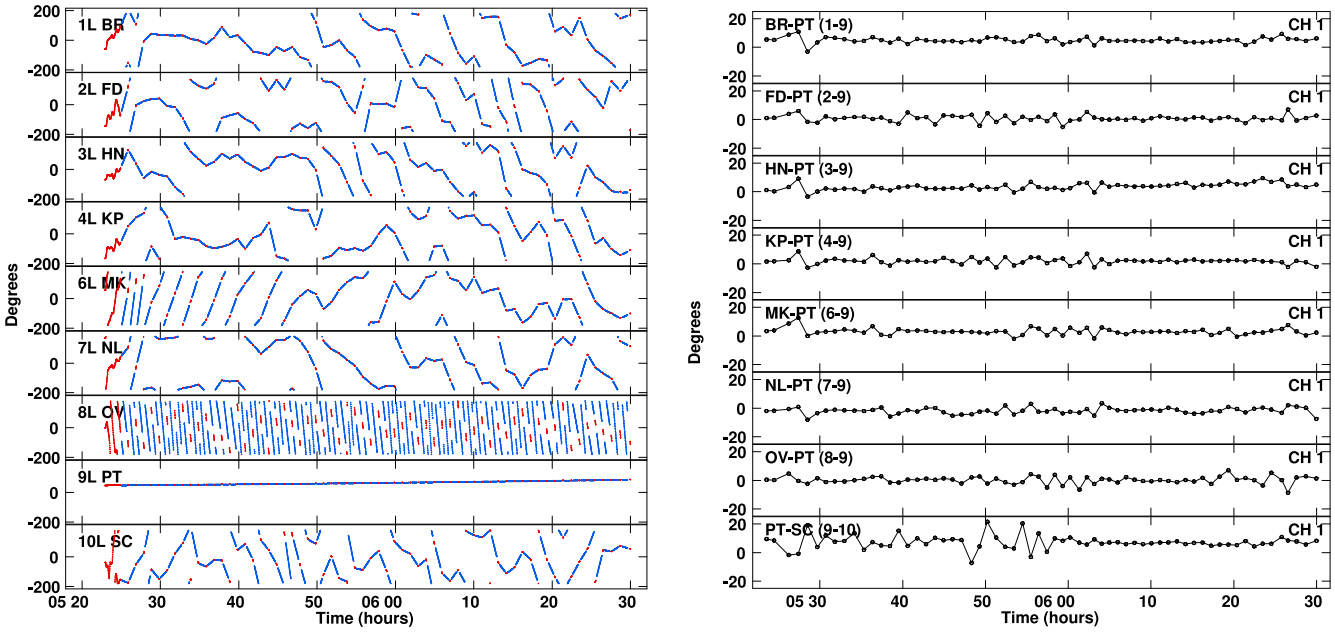

Figure 2. Left: final phase solutions at 43.2 GHz over the first observing hour during the first hour of observations. Red symbols denote the phase solutions of BL Lacertae, and blue symbols show the interpolated phases transferred from BL Lacertae to J2203+4208. Right: residual phases for BL Lacertae after application of the final phase solutions at 43.2 GHz during the same time interval.

Appendix B
Model-fitting Results

Figure 3 displays the CLEAN maps of J2203+4208 at all five frequencies. The peak SNRs in the CLEAN maps are approximately 47 at 8.4 GHz, 43 at 12.4 GHz, 39 at 15.2 GHz, 20 at 23.6 GHz, and 5.5 at 43.2 GHz. A single circular Gaussian model was adopted to fit the calibrated visibility data of J2203+4208 in order to determine its integrated flux densities and relative positions with respect to the reference position using the MODELFIT task. The results of model fitting for J2203+4208 are summarized in Table 3. We further fitted the total integrated flux densities of J2203+4208 with the model in Equation (1). The nonlinear least-squares optimization was performed using the `curve_fit` routine in the `SciPy` module, adopting the Levenberg–Marquardt algorithm. As shown in Figure 4, the fit yields an estimate of $S_0 = 140 \pm 6$ mJy.

Figure 5 yields the VLBA maps of BL Lacertae at five frequencies. We used the JMFIT task in AIPS to estimate the relative positional offset of peaks on the maps with respect to the correlation phase center coordinate for BL Lacertae. A model of a single elliptical Gaussian component was used. Table 4 reports the model-fitting results. The formal uncertainties on the positional offsets are typically $\lesssim$0.1 μas, which are not statistically meaningful and thus not listed in the table.

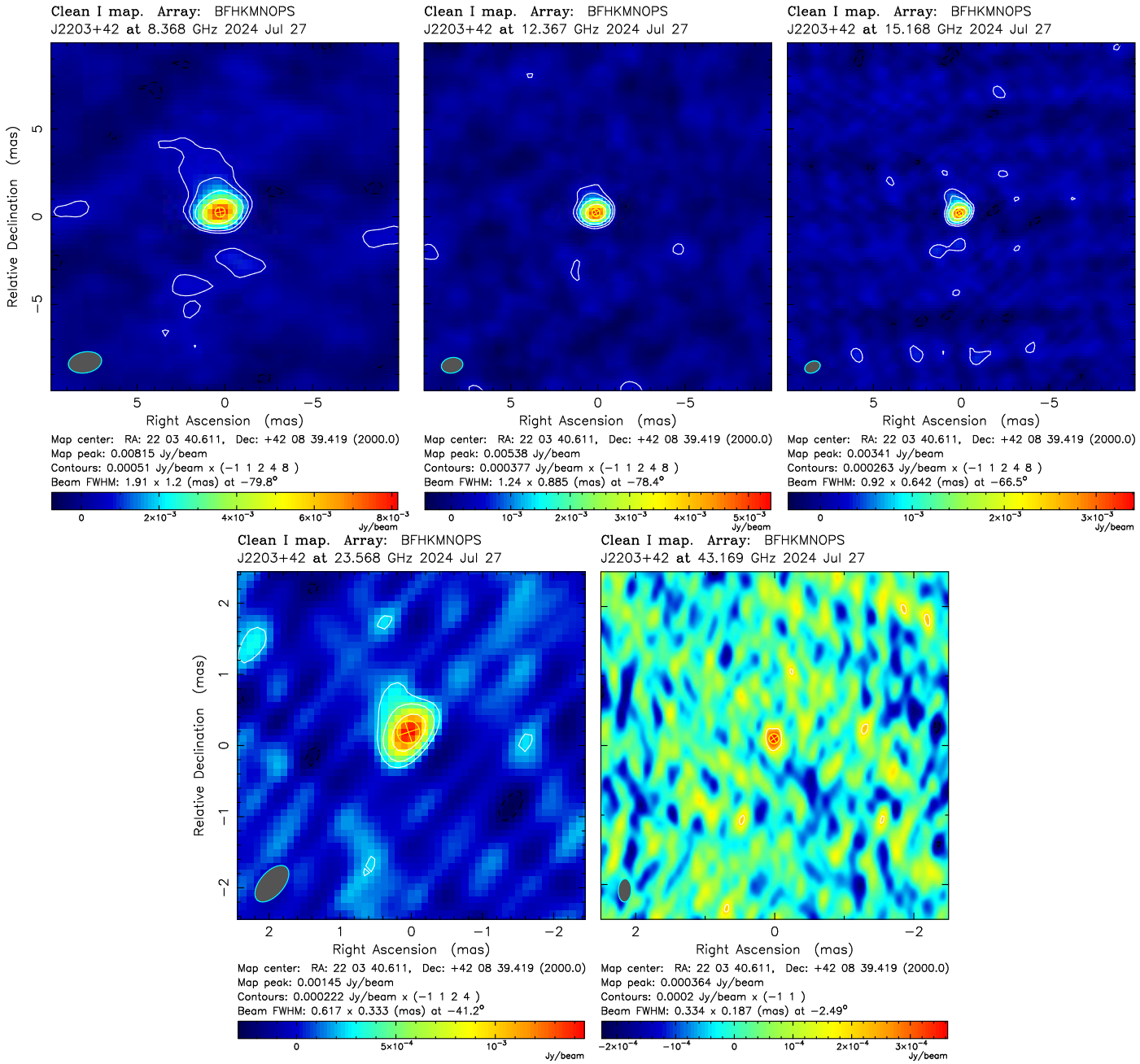

Figure 3. VLBA maps of J2203+4208 at 8.4, 12.4, 15.2, 23.6, and 43.2 GHz, respectively. The contours start from 3σ off-source noise level.

Table 3
Model-fitting Results of J2203+4208

Freq. (GHz)	$\Delta\alpha^*$ (μas)	$\Delta\delta$ (μas)	$S_{\rm int}$ (mJy)	$S_{\rm peak}$ (mJy beam^{-1})	FWHM (mas)
8.4	273 ± 4	267 ± 2	9.45 ± 0.04	8.15 ± 0.17	0.576
12.4	110 ± 6	230 ± 5	6.38 ± 0.08	5.38 ± 0.13	0.428
15.2	65 ± 8	208 ± 6	4.24 ± 0.09	3.41 ± 0.09	0.362
23.6	41 ± 13	188 ± 13	2.27 ± 0.13	1.45 ± 0.07	0.318
43.2	12 ± 22	98 ± 30	0.50 ± 0.12	0.36 ± 0.07	0.142

Note. The last column is the full width at half maximum.

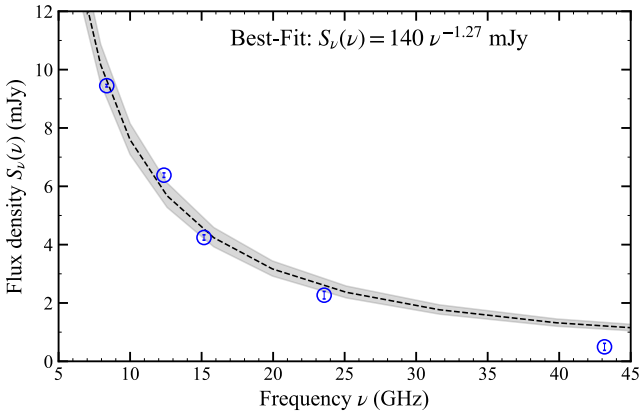

Figure 4. Radio spectrum of the reference source J2203+4208. The blue open circles denote the integrated flux densities obtained in this work, while the gray zone indicates the 1σ confidence interval.

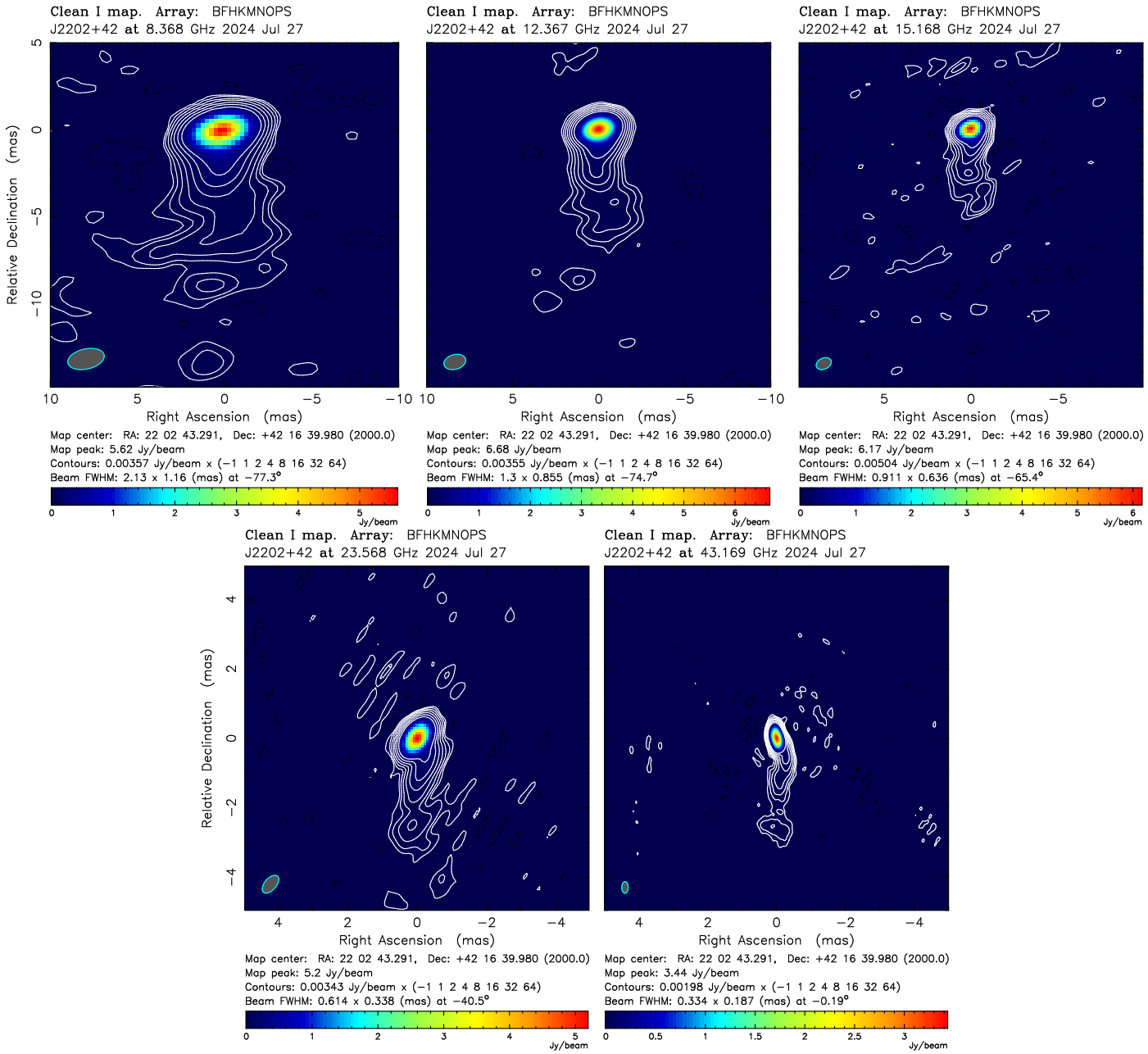

Figure 5. VLBA maps of BL Lacertae at 8.4, 12.4, 15.2, 23.6, and 43.2 GHz, respectively. The contours start from 3σ off-source noise level.

Table 4
Model-fitting Results of BL Lacertae

Freq. (GHz)	$\Delta\alpha^*$ (μas)	$\Delta\delta$ (μas)	$S_{\rm int}^{\rm core}$ (Jy)	$S_{\rm peak}$ (Jy beam^{-1})	a (mas)	b (mas)	ϕ (°)
8.4	174	−55	6.164 ± 0.002	5.680 ± 0.001	0.456	0.301	187
12.4	12	−12	7.098 ± 0.002	6.703 ± 0.001	0.300	0.062	205
15.2	3	−6	6.777 ± 0.004	6.256 ± 0.002	0.277	0.138	222
23.6	−1	9	6.546 ± 0.002	5.209 ± 0.001	0.265	0.076	207
43.2	5	10	5.615 ± 0.001	3.450 ± 0.001	0.346	0.052	205

Note. The formal uncertainties on the positional offsets are typically $\lesssim$0.1 μas. Here, a and b are the major and minor axes FWHM of the Gaussian component and ϕ is the position angle of the major axis of the component, measured north through east.

Appendix C
Core-shift Parameter Estimation

In the MCMC fitting, we used $N_{\rm walk} = 32$ walkers and ran each chain for $N_{\rm step} = 2 \times 10^5$ steps. The first $N_{\rm burn} = 2 \times 10^4$ steps were discarded as burn-in, and the remaining samples were used to construct the posterior probability distributions. For all parameters, the total chain length exceeds 50 $\tau_{\rm int}$, where $\tau_{\rm int}$ is the integrated autocorrelation time, indicating reliable convergence of the MCMC chains. We adopted the following priors: $0 < r_0 < 10$ mas, $0.1 < k_r < 10$, uniform priors on $(x_0,\ y_0)$ over $\pm$5 mas, and a uniform prior on the jet position angle of jet $\theta_J \in [0,\ 2\pi)$. Figure 6 presents the posterior probability distributions of all model parameters, revealing strong correlations (absolute Pearson correlation coefficients exceeding 0.4) among most parameters, except for the jet position angle.

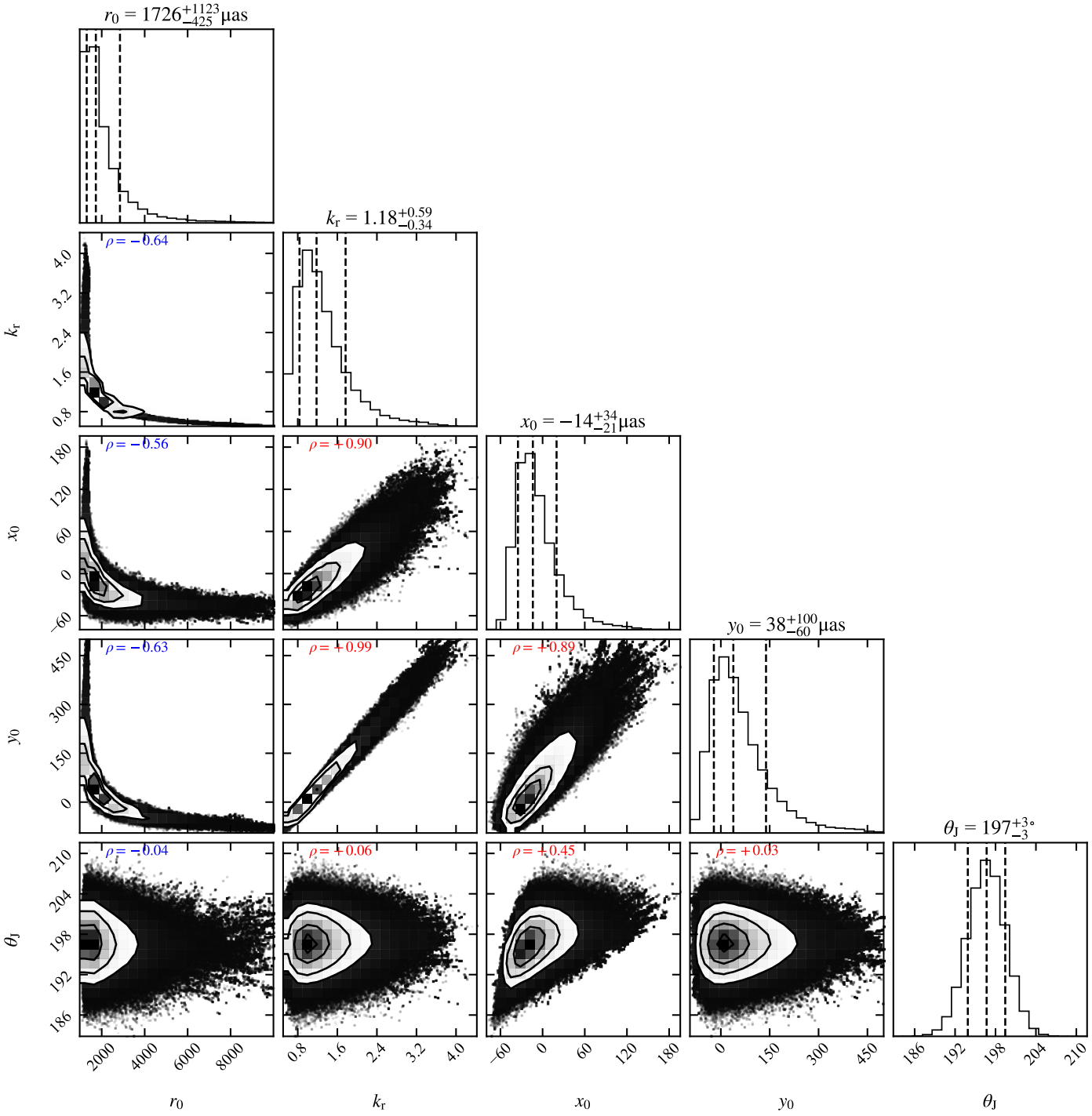

Figure 6. Posterior probability distributions of the core-shift parameters derived from the MCMC analysis. Pearson correlation coefficients between parameters are indicated, with red and blue denoting positive and negative correlations, respectively.

ORCID iDs

Niu Liu (刘牛) https://orcid.org/0000-0003-2778-002X
Jun Yang (杨军) https://orcid.org/0000-0002-2322-5232
Xiaopeng Cheng (程晓朋) https://orcid.org/0000-0003-4407-9868
Ai-Ling Zeng (曾艾玲) https://orcid.org/0009-0000-9427-4608
Wen Chen (陈文) https://orcid.org/0000-0002-5519-0628
Xiao-Long Yang (杨小龙) https://orcid.org/0000-0002-4439-5580
Xiaoyu Hong (洪晓瑜) https://orcid.org/0000-0002-1992-5260
Xia-Xuan Zhang (张夏轩) https://orcid.org/0009-0007-0631-291X
Jia-Cheng Liu (刘佳成) https://orcid.org/0000-0002-6637-9258

References

Agarwal, A., Mohan, P., Gupta, A. C., et al. 2017, MNRAS, 469, 813
Astropy Collaboration, Price-Whelan, A. M., Lim, P. L., et al. 2022, ApJ, 935, 167
Astropy Collaboration, Price-Whelan, A. M., Sipőcz, B. M., et al. 2018, AJ, 156, 123

Astropy Collaboration, Robitaille, T. P., Tollerud, E. J., et al. 2013, A&A, 558, A33
Blandford, R. D., & Königl, A. 1979, ApJ, 232, 34
Casadio, C., MacDonald, N. R., Boccardi, B., et al. 2021, A&A, 649, A153
Chamani, W., Savolainen, T., Ros, E., et al. 2023, A&A, 672, A130
Dodson, R., Rioja, M. J., Molina, S. N., & Gómez, J. L. 2017, ApJ, 834, 177
Foreman-Mackey, D., Hogg, D. W., Lang, D., & Goodman, J. 2013, PASP, 125, 306
Gómez, J. L., Lobanov, A. P., Bruni, G., et al. 2016, ApJ, 817, 96
Greisen, E. W. 2003, ASSL, 285, 109
Hada, K., Doi, A., Kino, M., et al. 2011, Natur, 477, 185
Hunter, J. D. 2007, CSE, 9, 90
Jorstad, S. G., Marscher, A. P., Lister, M. L., et al. 2005, AJ, 130, 1418
Jorstad, S. G., Marscher, A. P., Raiteri, C. M., et al. 2022, Natur, 609, 265
Kluyver, T., Ragan-Kelley, B., Pérez, F., et al. 2016, Positioning and Power in Academic Publishing: Players, Agents and Agendas (IOS Press), 87
Konigl, A. 1981, ApJ, 243, 700
Koss, M. J., Ricci, C., Trakhtenbrot, B., et al. 2022, ApJS, 261, 2
Lister, M. L., Aller, M. F., Aller, H. D., et al. 2018, ApJS, 234, 12
Lobanov, A. P. 1998, A&A, 330, 79
Marscher, A. 2010, in The Jet Paradigm: From Microquasars to Quasars, ed. T. Belloni (Springer), 173
Marscher, A. P., Jorstad, S. G., D'Arcangelo, F. D., et al. 2008, Natur, 452, 966
O'Sullivan, S. P., & Gabuzda, D. C. 2009, MNRAS, 400, 26
Petrov, L. 2024, The Radio Fundamental Catalog (National Aeronautics and Space Administration)
Petrov, L. Y., & Kovalev, Y. Y. 2025, ApJS, 276, 38
Planck Collaboration, Aghanim, N., Akrami, Y., et al. 2020, A&A, 641, A6
Plavin, A. V., Kovalev, Y. Y., Pushkarev, A. B., & Lobanov, A. P. 2019, MNRAS, 485, 1822
Pushkarev, A. B., Hovatta, T., Kovalev, Y. Y., et al. 2012, A&A, 545, A113
Rioja, M. J., & Dodson, R. 2020, A&ARv, 28, 6
Shepherd, M. C. 1997, ASPC, 125, 77
Sokolovsky, K. V., Kovalev, Y. Y., Pushkarev, A. B., & Lobanov, A. P. 2011, A&A, 532, A38
Van Der Walt, S., Colbert, S. C., & Varoquaux, G. 2011, CSE, 13, 22
Virtanen, P., Gommers, R., Oliphant, T. E., et al. 2020, NatMe, 17, 261
Zamaninasab, M., Clausen-Brown, E., Savolainen, T., & Tchekhovskoy, A. 2014, Natur, 510, 126